Bull. Mater. Sci., Vol. 39, No. 1, February 2016, pp. 133–145. © Indian Academy of Sciences.

Nanohydroxyapatite synthesis using optimized process parameters for load-bearing implant

FEVEN MATTEWS MICHAEL[1], M KHALID[1,*], C T RATNAM[2], W RASHMI[3], M E HOQUE[4] and MOHAMMAD REZA KETABCHI[1]

[1]Division of Manufacturing and Industrial Processes, Faculty of Engineering, University of Nottingham Malaysia Campus, Jalan Broga, 43500 Semenyih, Selangor, Malaysia
[2]Radiation Processing Technology Division, Malaysian Nuclear Agency, Bangi, Selangor, Malaysia
[3]Energy Research Group, School of Engineering, Taylor's University, 47500 Subang Jaya, Selangor, Malaysia
[4]Department of Biomedical Engineering, King Faisal University Al-Hofuf, Al-Ahsa 31982, Kingdom of Saudi Arabia

MS received 9 June 2015; accepted 14 September 2015

Abstract. In this study, nanohydroxyapatite (NHA) was synthesized using calcium nitrate tetrahydrate and diammonium hydrogen phosphate via the precipitation method assisted with ultrasonication. Three independent process parameters: temperature (*T*) (70, 80 and 90°C), ultrasonication time (*t*) (20, 25 and 30 min), and amplitude (*A*) (60, 65 and 70%) were studied and optimized using response surface methodology based on 3 factors and 5 level central composite design. The responses of the model were analysed with the help of the particle size measured from field-emission scanning electron microscopy and Brunauer–Emmett–Teller (BET). The surface area of particle was measured with BET and the thermal stability of the powder was measured using thermogravimetric analysis. Finally, with the optimized process parameters obtained from the model, the NHA powder was synthesised and validated against the predicted value. The results show a good agreement with an average error 8% between the actual and predicted values. Moreover, the thermal stability and porosity of synthesized NHA was further improved after calcination. This improvement could be due to the removal of impurities from the NHA powder after calcination as indicated by the Fourier transform infrared spectroscopy and energy-dispersive X-ray spectroscopy.

Keywords. Nanohydroxyapatite; ultrasonication; response surface methodology; calcination; optimization.

1. Introduction

Nanohydroxyapatite (NHA) $Ca_{10}(PO_4)_6(OH)_2$, a major constituent of the inorganic segment of human bone [1,2], is a bioceramic material that can easily be synthesized. However, the morphological, thermal stability, and chemical properties of this NHA powder can be greatly influenced by the technique used and by modulating the conditions of the synthesis [3]. So far, the most reported technique used to synthesize NHA is the direct precipitation method, which is considered to be simple and cost effective. Nonetheless, the quality of the powder synthesized is poor due to the formation of agglomerated particles [4]. This limitation can be overcome with the help of ultrasonication, where the agglomerates can be broken down into smaller sizes and homogeneously dispersed [5]. From many studies conducted [6], calcination of the NHA powder has shown to improve the homogeneous dispersion of the powder and further enhances the densification of the powder due to increase in surface area. This in turn, improves the mechanical properties of the synthesized NHA powder. Moreover, calcination has also proved to improve the quality of the NHA powder by removing the impurities that could be present either during synthesize or due to environmental reaction [7].

In this study, NHA powder was synthesized using the precipitation technique accompanied by ultrasonication. The influence of different ultrasonication parameters on the properties of NHA powder was studied by varying the ultrasonic time and amplitude as well as the temperature of the solution. The uniqueness of this study is the application of response surface methodology (RSM), which is an effective statistical technique used to optimize the process parameters having three or more factors [8]. The advantage of using RSM is the reduction in the number of experimental runs needed to evaluate multiple process parameters and their interaction. In addition, it is more efficient, easier to arrange and interpret the experimental results compared with others. Therefore, in this study central composite design (CCD), one of the RSMs based on 3 factors and 5 level designs is used to obtain the optimum condition to synthesize NHA powder. This analysis was based on the thermal stability, particle size and surface area of the NHA powder. Finally, the effect of calcination on the NHA powder was also investigated by calcinating the NHA powder synthesized at the optimum condition.

*Author for correspondence (khalid.siddiqui@nottingham.edu.my)

2. Materials and methodology

2.1 *Materials*

The chemicals used to synthesize NHA such as di-ammonium hydrogen phosphate (A.P.), calcium nitrate tetrahydrate (C.P.), ammonium solution (30%) (A.P.), and absolute alcohol 99.7% (denatured) (A.P.) were purchased from LGC Scientific, Malaysia. Hydroxyapatite nanopowder (≥97% and <200 nm (Brunauer–Emmett–Teller (BET))) used for comparison purpose was purchased from Sigma-Aldrich. All chemicals were analytical grades and were used without further modification.

2.2 *Sample preparation*

A solution of 50 ml of 1 M calcium nitrate tetrahydrate and 35 ml of 0.6 M diammonium hydrogen phosphate was prepared with the assistance of ultrasonication (Cole Palmer ultrasonic processor). The pH of the solution was adjusted with ammonium solution. After the reactions were completed, the solutions were vacuum filtered and washed with water and ethanol. The washed precipitates (NHA) were collected and kept in the hot air oven to dry at 70°C for overnight. The dried NHA powder was then used for further characterization.

2.3 *Characterization tests*

2.3a *BET*: The specific surface area of the powder was then determined using BET (micromeritics ASAP 2020 surface area and porosity analyser). The powdered samples were degassed using a Unit 1—S/N: 720, port 1 at 300°C for 1 h prior to analyses. BET analysis provides a precise specific surface area from which the particle size of synthesized NHA was calculated. Based on the theoretical density (3.156 g cm^{-3}) of NHA [9], the particle size was calculated using

$$D\ (\text{nm}) = \frac{6}{S_w \rho_w}. \tag{1}$$

2.3b *Thermogravimetric analysis (TGA)*: The thermal degradation of the synthesized NHA was measured using a thermogravimetric analyzer (TGA, Mettler Toledo TGA/DSC 1 equipped with STAR^e System). Less than 15 mg of NHA powder was heated at 10°C min^{-1} from room temperature to 1000°C. The analysis was conducted under nitrogen atmosphere at a constant flow rate of 10 ml min^{-1}, in order to avoid unwanted oxidation.

2.3c *Field-emission scanning electron microscope (FESEM)*: The particle size and elemental composition of the powder were examined using FESEM (FEI Quanta 400). The sample was subjected to low vacuum at an accelerating voltage of 20 kV, current of 60–90 mA and working distance of about 8.2 mm. An average of few measurements of the particle size was taken and standard deviation was calculated.

2.3d *Fourier transform infrared (FTIR) spectroscopy*: The chemical functional group of the NHA powder was characterized using FTIR spectroscopy (Perkin Elmer Spectrum 2000). The spectrometer was operated with 50 scans at 4 cm^{-1} resolution and within the range of 4000–400 cm^{-1} for each sample. All FTIR spectra were recorded in absorbance unit. The test was conducted by preparing a disk from a mixture of NHA and KBr at a weight ratio of 0.2–1%.

2.3e *X-ray diffraction (XRD)*: XRD patterns for the NHA powder samples were collected by Panalytical X'Pert Pro model using Cu-K_α radiation ($\lambda = 0.15418$ nm). Data were collected over the range of 2θ values from 15° to 80° with step size of 0.2° and stop time of 2.5 s.

2.3f *Transmission electron microscope (TEM)*: The morphology and the particle size of the synthesized NHA powder were evaluated using TEM (Jeol-JEM-2100). The sample was prepared by dispersing the NHA powder into ethanol using 1 h sonication. Later, the samples were observed under TEM using a voltage of 200 kV.

2.3g *Zeta-sizer*: The particle size distribution of the NHA powder was measured using Zeta-sizer (ZS, Malvern Zetasizer nano). The sample was prepared by dispersing the NHA powder into water using sonication for 1h. A drop of the prepared sample was then diluted with distilled water in the disposable cuvette and measured.

2.4 *Experimental design and statistical analysis*

The optimization of ultrasonication-related process parameters to synthesize NHA powder was conducted using response surface methodology (RSM). The experiment was carried out with the help of central composite design (CCD) with 3 factors and 5 levels as shown in table 1. The three independent parameters used for this study are temperature of the solution (T) (70–90°C), ultrasonic time (t) (20–30 min), and amplitude, i.e., ultrasonic power (A) (60–70%). The complete design consisted of 20 runs, where run 15–20 were used to evaluate the pure error whereas runs 13 and 14

Table 1. Independent parameters used in CCD for NHA synthesis.

	Levels				
Parameters/factors	$-\alpha$	-1	0	$+1$	$+\alpha$
Temperature	63.18	70	80	90	96.82
Ultrasonic time	16.59	20	25	30	33.41
Amplitude	56.59	60	65	70	73.41

were outliers. The responses chosen to optimize the parameters are particle size measured from both FESEM and BET, surface area measured by BET and the weight loss or thermal degradation measured by the TGA. The data collected in table 2, were analysed using multiple regressions to fit the quadratic polynomial model. Once the optimum conditions were determined, the NHA powder was synthesized again using the optimum conditions. The NHA powder was then calcinated at 800°C for 2 h and further characterized using TGA, XRD, FTIR, Zeta-sizer, TEM, EDX, and FESEM for comparison with the NHA powder before calcination.

3. Results and discussion

3.1 *Modelling of NHA characterization*

Table 2 shows the process variables and experimental data obtained after conducting the characterization tests. The statistical testing of the model was performed in the form of analysis of variance (ANOVA) where the fitted quadratic polynomial model of the characterization tests is summarized in table 3. Through multiple regression analysis on the experimental data, the model for the predicted responses of particle size (FESEM) (Y_1), particle size (BET) (Y_2), surface area (Y_3), and the remaining weight (Y_4) could be expressed by the following quadratic polynomial equations in terms of coded factors as shown in equations (2)–(5), respectively, where A = temperature, B = time, and C = amplitude:

$$\begin{aligned} Y_1 &= 127.34 + 7.22A + 4.64B + 0.26C \\ &\quad +16.14A^2 + 18.35B^2 - 0.87C^2 \\ &\quad -2.10AB + 2.80AC - 15.34BC, \end{aligned} \tag{2}$$

$$\begin{aligned} Y_2 &= 25.42 + 4.11A + 3.85B + 0.016C \\ &\quad -3.30A^2 + 8.69B^2 - 2.22C^2 \\ &\quad -0.50AB - 5.13AC - 2.27BC, \end{aligned} \tag{3}$$

$$\begin{aligned} Y_3 &= 77.33 - 9.93A - 6.39B - 2.31C \\ &\quad +13.50A^2 - 19.72B^2 - 0.43C^2 \\ &\quad +1.76AB + 12.21AC + 3.07BC, \end{aligned} \tag{4}$$

$$\begin{aligned} Y_4 &= 65.04 - 3.68A - 9.95B - 2.31C \\ &\quad -11.62A^2 - 0.25B^2 + 9.83C^2 \\ &\quad +2.24AB + 4.68AC + 4.35BC. \end{aligned} \tag{5}$$

From table 3, the determination coefficient (R^2) for particle size (FESEM and BET), surface area (BET), and weight remaining (TGA) were 0.9659, 0.9148, 0.9076, and 0.9547, respectively. This implies that 96.59, 91.48, 90.76 and 95.47% of the variations could be explained by the fitted model. For a good statistical model, R^2 adj should be close to R^2 where the R^2 adj for particle size (FESEM and BET), surface area (BET) and weight remaining (TGA) was 0.9044, 0.7615, 0.7413 and 0.8732, respectively. This in turn would mean that only 9.56, 23.85, 25.87 and 12.68% of the total variations were not explained by the model.

Table 2. Factors and levels for CCD experimental design and their actual and predicted results.

Run	Temperature (°C)	Time (min)	Amplitude (%)	FESEM—particle size (nm)		BET—particle size (nm)		BET—surface area ($m^2\ g^{-1}$)		TGA—wt remaining (wt%)	
				Actual	Predicted	Actual	Predicted	Actual	Predicted	Actual	Predicted
1	70	30	60	165.017	170.11	19.169	21.69	99.0501	93.34	65.776	63.68
2	90	20	60	136.088	138.99	26.344	27.91	72.0744	67.98	76.7873	75.55
3	90	30	70	152.713	157.08	26.088	28.00	72.7812	69.54	63.6909	61.97
4	80	33.41	65	153.338	148.97	39.21	37.30	48.425	51.67	56.7622	58.48
5	90	20	70	187.79	182.70	28.365	25.84	66.9387	72.65	66.5943	68.69
6	70	20	70	156.275	158.46	25.927	26.88	73.2326	71.61	72.021	71.16
7	70	20	60	150.73	146.36	20.953	19.04	90.6207	93.86	74.1495	75.87
8	80	16.59	65	148.85	153.22	34.677	36.59	54.7545	51.51	62.1142	60.39
9	80	25	56.59	139.82	138.38	30.732	29.51	61.7831	66.72	62.0851	62.84
10	80	25	73.41	137.46	138.90	28.319	29.54	67.0476	62.11	58.9614	58.21
11	70	30	70	142.95	140.04	31.881	30.31	59.5572	63.65	54.7941	56.03
12	90	30	60	182.62	180.44	42.995	42.04	44.1613	45.78	48.2089	49.07
13	63.18	25	65	188.26	—	25.43	—	74.666	—	75.5886	—
14	96.82	25	65	158.47	—	36.127	—	52.557	—	64.0314	—
15–20	80	25	65	123.08	124.78	23.194	24.03	81.8621	79.96	69.9123	69.21

Table 3. Analysis of variance for the fitted quadratic model of the characterization of NHA synthesized.

Source	FESEM—particle size (nm)					BET—particle size (nm)					BET—surface area ($m^2\ g^{-1}$)					TGA—wt remaining (wt%)				
	SS	DF	MS	*F*-value	*p*-value	SS	DF	MS	*F*-value	*p*-value	SS	DF	MS	*F*-value	*p*-value	SS	DF	MS	*F*-value	*p*-value
Model	5876	9	652.9	15.72	0.0037	536.5	9	59.61	5.97	0.0317	2655.9	9	295.1	5.46	0.038	733.7	9	81.52	11.71	0.0072
Residual	207.7	5	41.54			49.96	5	9.99			270.40	5	54.08			34.80	5	6.96		
Lack of fit	207.7	2	103.8			49.96	2	24.98			270.40	2	135.2			34.80	2	17.40		
Pure error	0	3	0			0	3	0			0	3	0			0	3	0		
Cor. total	6983	17				689	17				3599.9	17				921.6	17			
	$R^2 = 0.9659$, Adj $R^2 = 0.9044$, C.V. = 4.48					$R^2 = 0.9148$, Adj $R^2 = 0.7615$, C.V. = 11.52					$R^2 = 0.9076$, Adj $R^2 = 0.7413$, C.V. = 10.17					$R^2 = 0.9547$, Adj $R^2 = 0.8732$, C.V. = 4.02				

However, the reliability and correlation between the actual and predicted values are indicated by the coefficient of variance (CV). From table 3, the relatively low CV values for particle size (FESEM) (4.48%), particle size (BET) (11.52%), surface area (BET) (10.17%), and weight remaining (TGA) (4.02%) indicate high degree of correlation between the actual and predicted values. Furthermore, the significance of the model was also analysed by the F-value and p-value as shown in table 3. This is because, the R^2 and CV values become more significant if the F-value is greater and p-value is less. As a result, the F-value and p-value of the model for particle size (FESEM and BET), surface area (BET), and weight remaining (TGA) were 15.72 and 0.037, 5.97 and 0.0317, 5.46 and 0.0381, and 11.71 and 0.0072, respectively. This implies that the model is significant since all the p-values are less than 0.05.

3.2 *Analysis of response surface*

Figures 1–4 depict the relationship between the independent and dependent variables by a 3-D representation of the response surfaces and 2-D contours generated by the model. Generally, contour plots relate the different interactions between the variables, indicating the significance of the interactions between the variables. The 3-D response surfaces on the other hand indicate the direction in which the original design must be placed to reach optimal conditions. These response surfaces are characterized based on their points located within the experimental regions, for instance as either maximum, minimum, or saddle [8]. Saddle points are inflexion points between relatively maximum and minimum points. In this case, increasing or decreasing both variables at the same time will lead to a decrease in response. But, increasing one variable while decreasing the other will increase in the response.

Table 4 summarizes the descriptions of the response surfaces and contour plots of the model. As a result, the 3-D response surfaces, from figure 1 showed minimum points located within the experimental regions for all variable interactions. However, figures 2–4 show maximum points located within the experimental regions especially for combinations of temperature and amplitude, amplitude and time, as well as time and temperature, respectively. For the rest of variable interactions, figures 2–4 present saddle points. That being said, the contour plots for all the variables showed significant interaction between each other. These were further complemented with the p-values obtained from the quadratic model, which were 0.0455, 0.0277, 0.0215 and 0.0242 for particle size (FESEM and BET), surface area (BET) and weight remaining (TGA), respectively.

3.3 *Optimization of process parameters*

The optimum process parameters for synthesize of NHA powder were determined from the 3-D plots and their respective contour plots. The predicted values for the particle size (FESEM and BET), surface area (BET) and weight

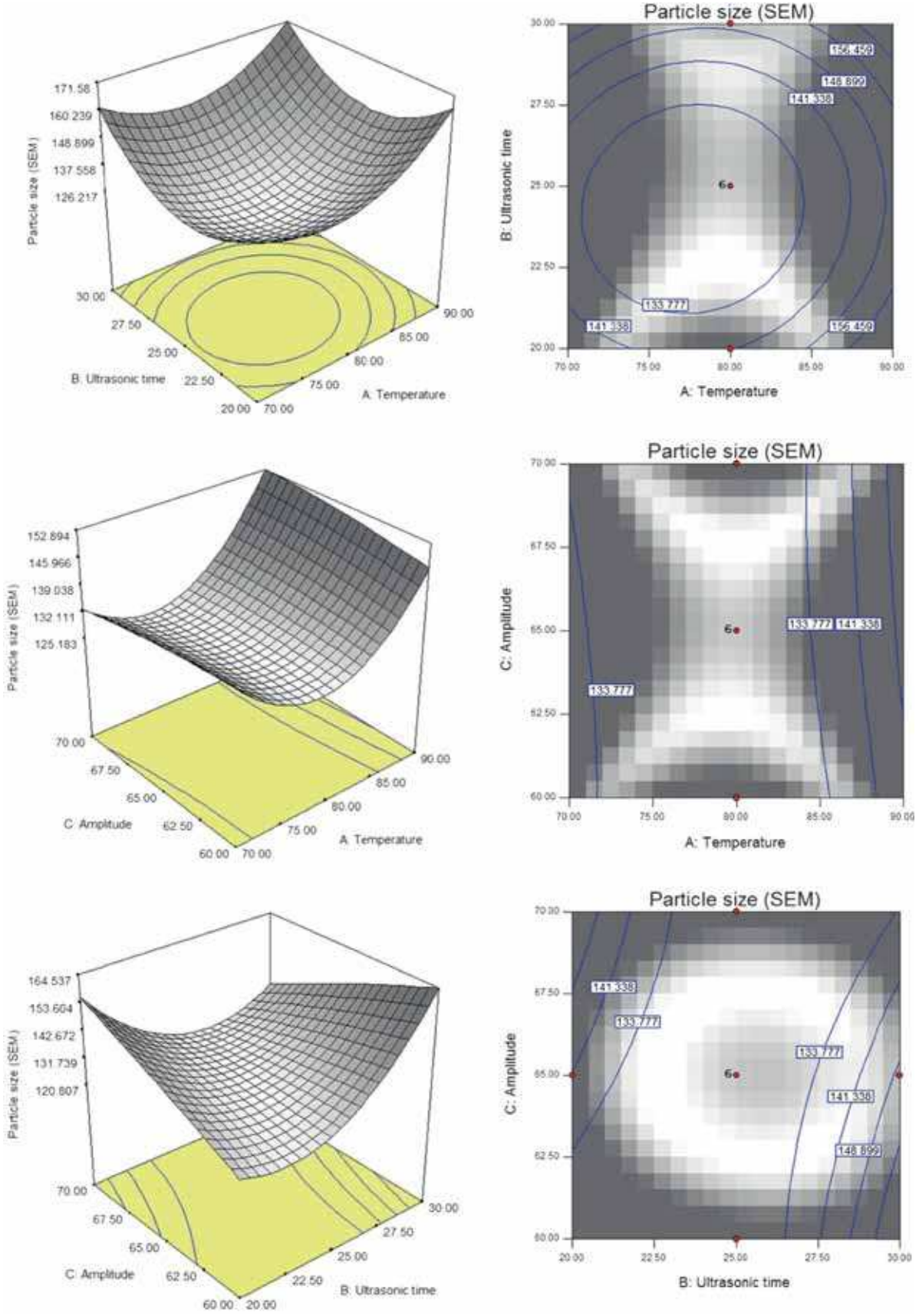

Figure 1. Response surface plot and contour plot of temperature of solution, ultrasonic time, and amplitude and their effect on the particle size of NHA measured through FESEM.

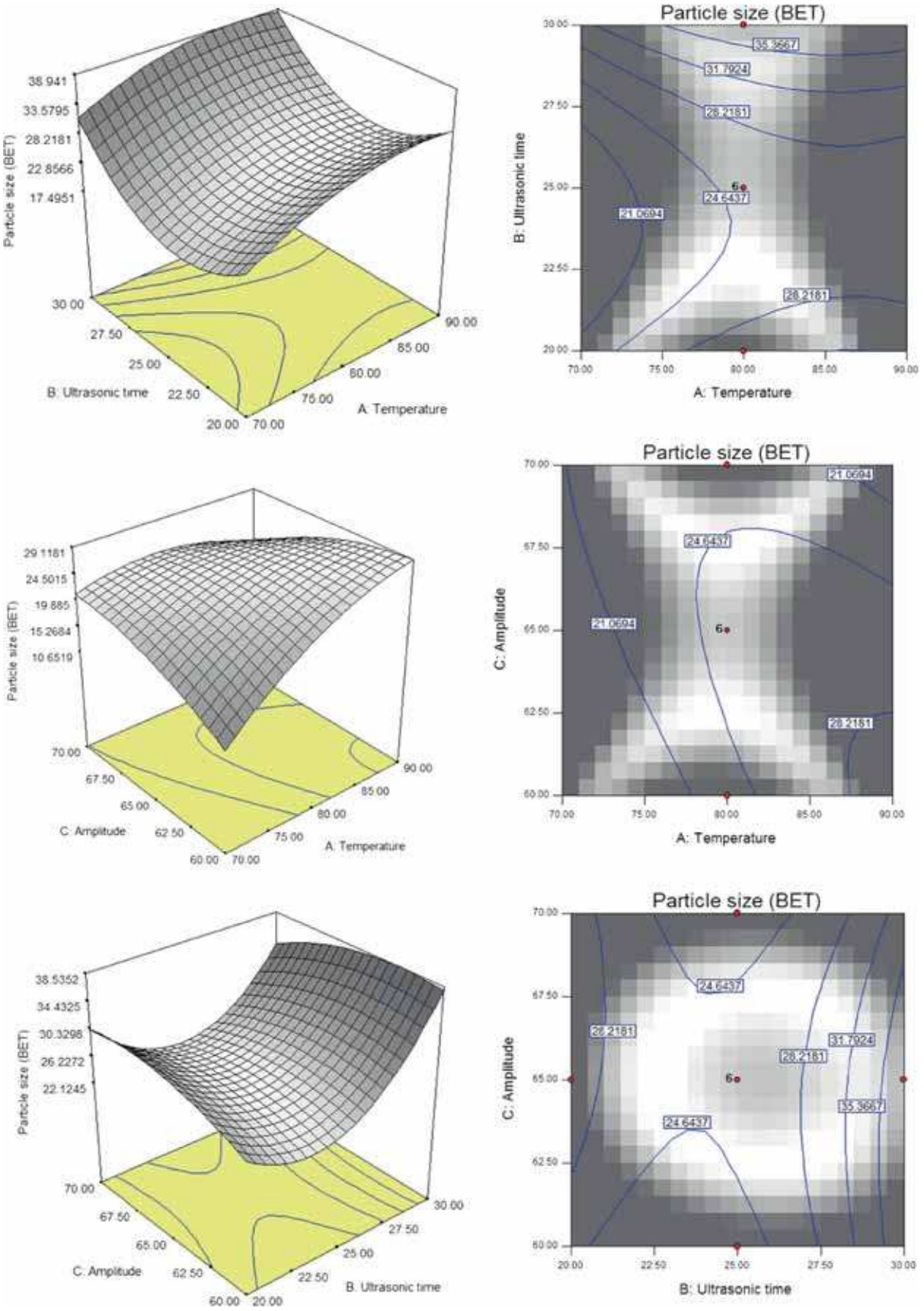

Figure 2. Response surface plot and contour plot of temperature of solution, ultrasonic time, and amplitude and their effect on the particle size of NHA measured through BET.

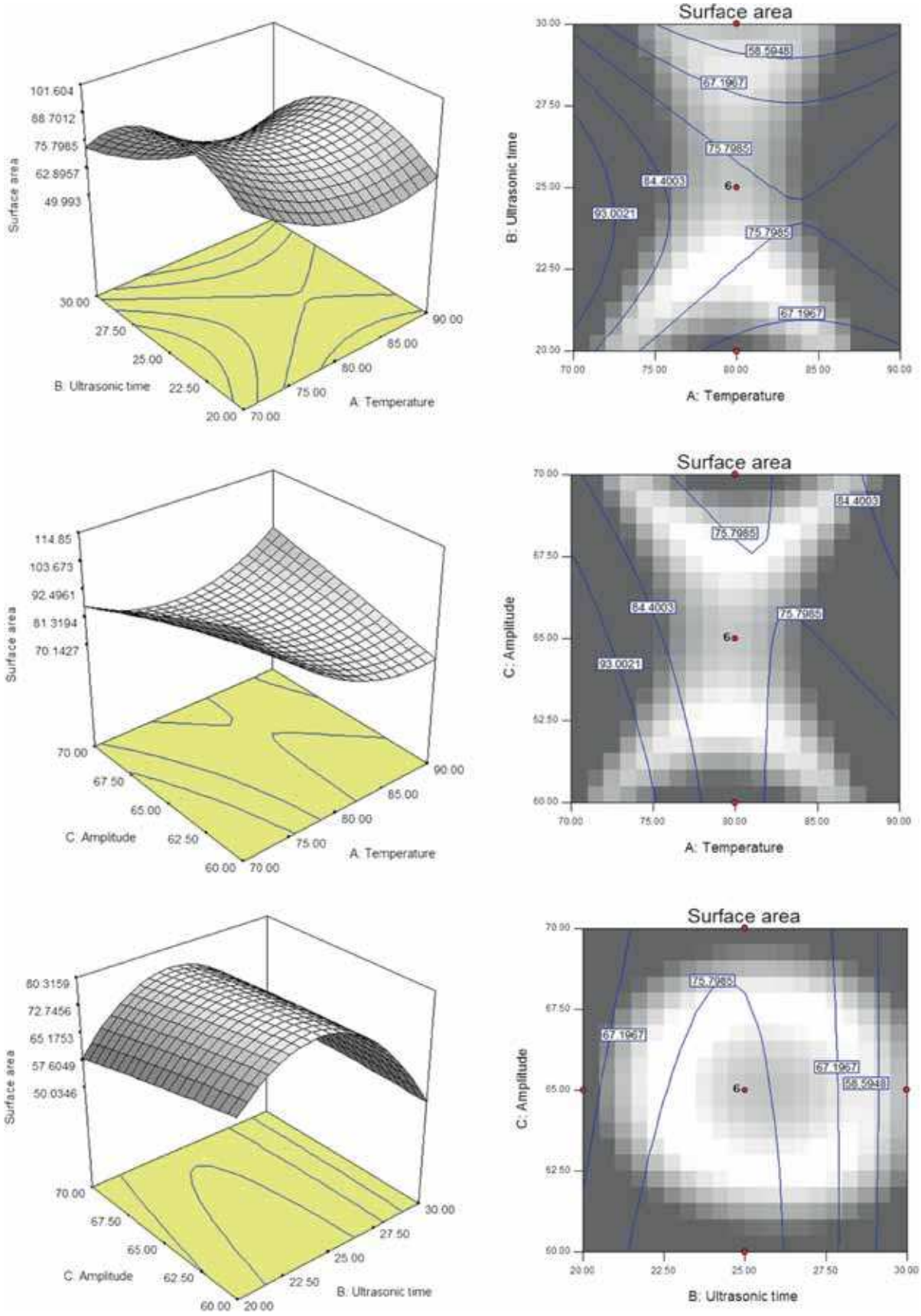

Figure 3. Response surface plot and contour plot of temperature of solution, ultrasonic time, and amplitude and their effect on the surface area of NHA measured through BET.

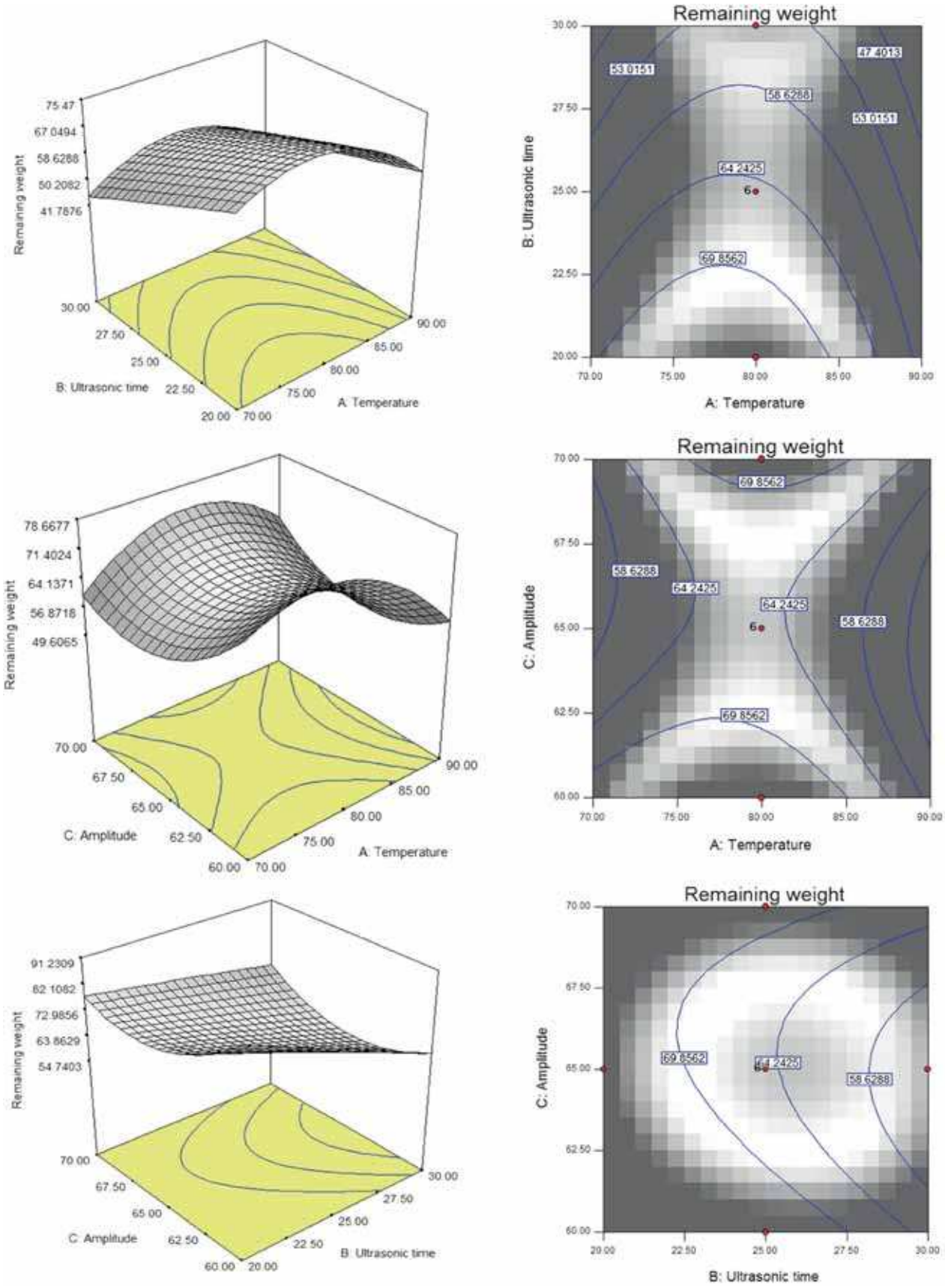

Figure 4. Response surface plot and contour plot of temperature of solution, ultrasonic time, and amplitude and their effect on the weight loss of NHA after TGA analysis.

Table 4. Summarized description of the response surfaces and contour plots.

Figures	Variable interaction	Response surface plot	Contour plot
1	Ultrasonic time *vs.* temperature	Minimum point located inside the experimental region	Simple circular pattern—significant interaction
	Amplitude *vs.* temperature	Minimum point located inside the experimental region	Stationary ridge pattern—significant interaction
	Amplitude *vs.* ultrasonic time	Minimum point located inside the experimental region	Stationary ridge pattern—significant interaction
2	Ultrasonic time *vs.* temperature	Saddle points—inflexion points between relatively maximum and minimum	Eclipse with minimax pattern—significant interaction
	Amplitude *vs.* temperature	Maximum point located inside the experimental region	Eclipse pattern—significant interaction
	Amplitude *vs.* ultrasonic time	Saddle points which are inflexion points between relatively maximum and minimum	Eclipse with minimax pattern—significant interaction
3	Ultrasonic time *vs.* temperature	Saddle points which are inflexion points between relatively maximum and minimum	Eclipse with minimax pattern—significant interaction
	Amplitude *vs.* temperature	Minimum point located inside the experimental region	Eclipse with minimax pattern—significant interaction
	Amplitude *vs.* ultrasonic time	Maximum point located inside the experimental region	Eclipse with minimax pattern—significant interaction
4	Ultrasonic time *vs.* temperature	Maximum point located inside the experimental region	Eclipse with rising ridge pattern—significant interaction
	Amplitude *vs.* temperature	Saddle points which are inflexion points between relatively maximum and minimum	Eclipse with minimax pattern—significant interaction
	Amplitude *vs.* ultrasonic time	Minimum point located inside the experimental region	Eclipse with rising ridge pattern—significant interaction

Table 5. Optimized conditions and the predicted and actual value of the responses at optimum conditions.

	Temperature (°C)	Time (min)	Amplitude (%)	FESEM—particle size (nm)	BET—particle size (nm)	BET—surface area ($m^2\ g^{-1}$)	TGA—wt remaining (wt%)
Predicted value	76.26	23.52	61.43	123.775	20	88.6316	76.7871
Actual value	75	23.52	61	132.9526	20.16	94.1963	72.0847
Percentage error	1.7	0	0.7	−7.4	−0.8	−6.3	6.1

remaining (TGA) at the predicted optimum process parameters are shown in table 5. These predicted values were compared with the actual value by synthesizing the NHA powder at the optimum process parameters. However, considering the operability of the ultrasonication machine in the actual process, the parameters were modified from $T = 76.26$°C, $t = 23.52$ min, and $A = 61.43\%$ to $T = 75$°C, $t = 23.52$ min, and $A = 61\%$. Therefore, the results obtained based on the modified process parameters were almost similar to the predicted values as the percentage errors were less than $\pm 8\%$ as shown in table 5.

3.4 *Properties of the synthesized NHA powder*

Figures 5 and 6 depict the thermal stability of the synthesized NHA at the optimum parameters using TGA thermogram. From figure 5, three stages of degradation as a result of absorbed and lattice water removal and dehydroxylation of the NHA powder can be observed. These degradation stages take place at 25–100, 200–400 and beyond 500°C, respectively [10,11]. The removal of the absorbed water is reversible therefore, even after calcination, there is still water removed at 25–100°C unlike the lattice water. Moreover, the thermal stability of the NHA powder was improved by 26.35% after calcination as shown in figure 6. This is because, the formation of oxyapatite as a result of hydroxyapatite deformation, is eliminated. This is further supported by the XRD pattern shown in figure 7, where the slight shift from $2\theta = 27°$ to 26° and broadening of the peak after calcination indicates the presence of more of hydroxyapatite rather than oxyapatite [12]. In addition, the crystallinity of the NHA powder was improved after calcination as reflected in figure 7, where the peaks became sharper with higher intensity compared with the NHA before calcination. FTIR spectrum and EDX of the synthesized NHA powder are shown in figures 8 and 9, respectively. From the FTIR spectra in figure 8, two peaks for stretching and bending modes of P–O are identified at 1029.93 and 603.52 cm^{-1}, respectively, indicating the presence of PO_3^{4-} ions [6,9]. Furthermore, at wavelength of 825 cm^{-1} presence of acidic phosphate group

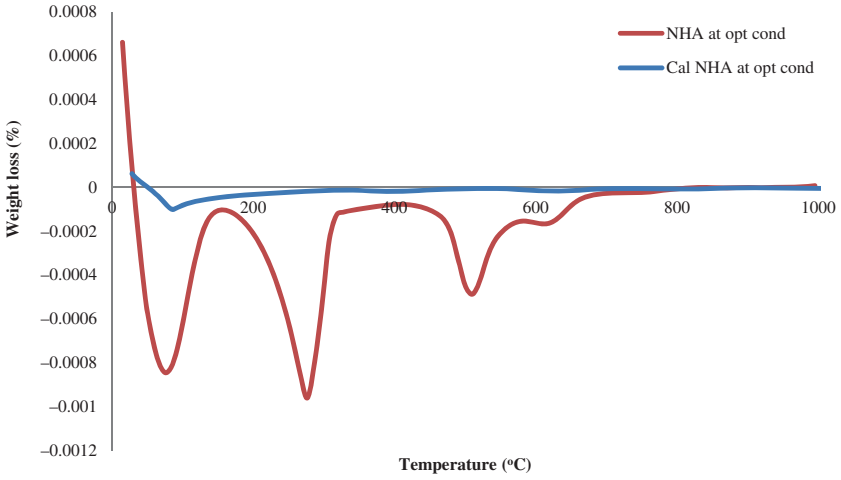

Figure 5. DTGA result for the NHA synthesized at the optimized condition before and after calcination.

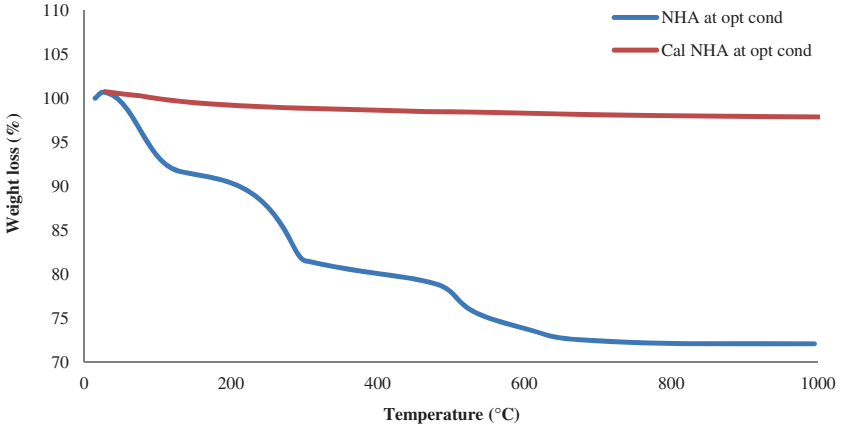

Figure 6. TGA result for the NHA synthesized at the optimized condition before and after calcination.

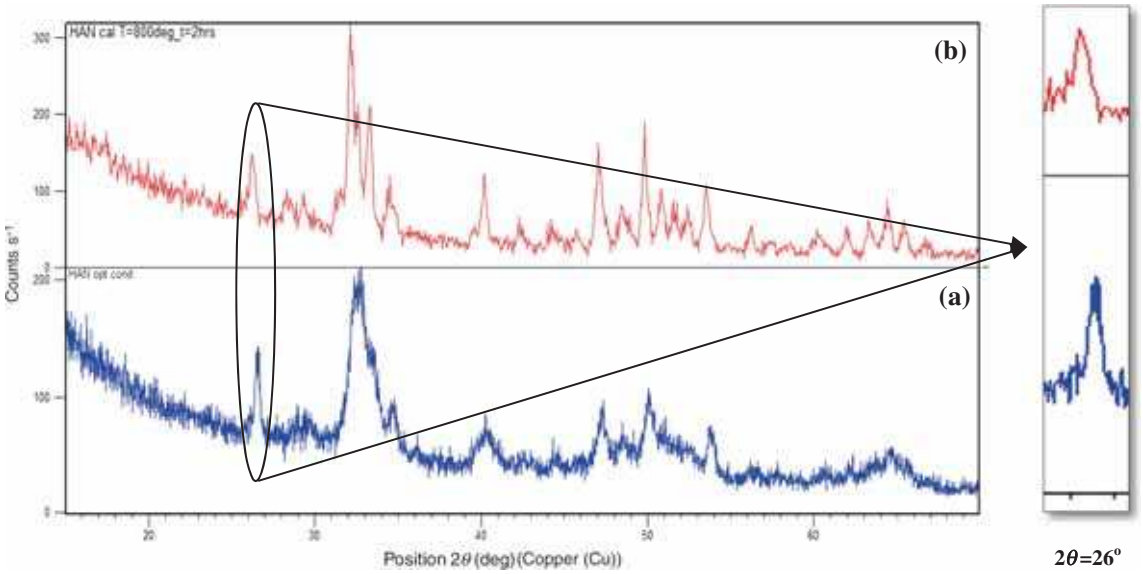

Figure 7. XRD patterns for the NHA synthesized at the optimized condition (**a**) before calcination and (**b**) after calcination.

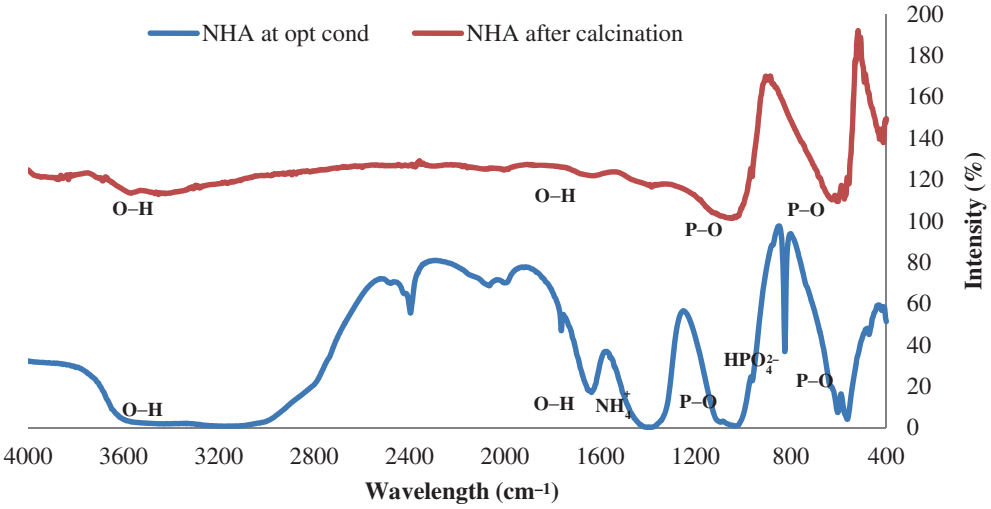

Figure 8. FTIR spectrum for the NHA synthesized at the optimized condition before calcination and after calcination.

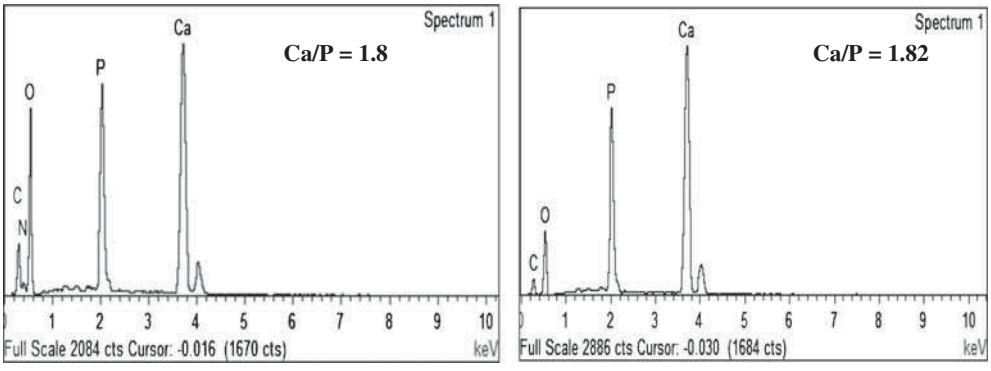

(a) **(b)**

Figure 9. EDX result obtained for the NHA synthesized at the optimized condition (**a**) before calcination and (**b**) after calcination.

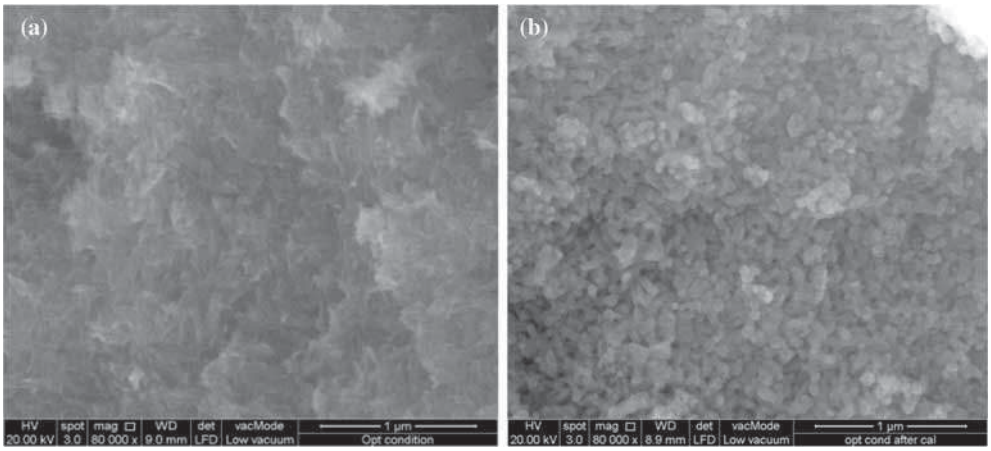

Figure 10. FESEM image for the NHA synthesized at the optimized condition (**a**) before calcination and (**b**) after calcination.

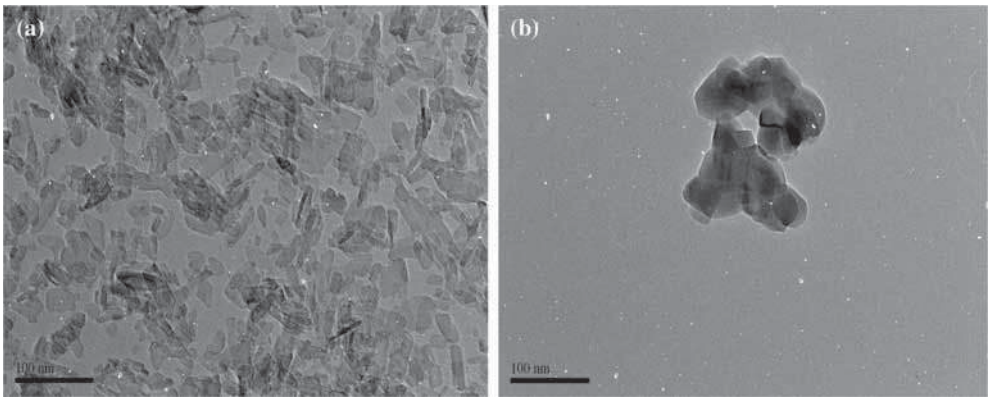

Figure 11. TEM image for the NHA synthesized at the optimized condition (**a**) before calcination and (**b**) after calcination.

(HPO_4^{2-}) were detected for uncalcinated NHA. Other peaks shown at 1636.43 and 3138.29 cm^{-1} indicates presence of O–H ions in the NHA powder [11]. Furthermore, the presence of nitrate group was detected at band width of 1393.88 cm^{-1} [11]. This is complimented with the EDX result obtained in figure 9a, where the presence of nitrogen element is detected due to the ammonium solution used during the synthesize of NHA to adjust the pH of the solution. However, the FTIR spectrum and EDX results in figures 8 and 9b, respectively, show complete removal of the impurities that is the nitrate group after the NHA powder was calcinated. The intensities of O–H functional groups are seen to decrease after calcination, indicating water loss occurred [7]. However the P–O ions remain unchanged even after the powder was calcinated. Furthermore, the Ca/P ratio as shown in figure 9 shows no significant changes in the synthesized NHA powder before and after calcination, which was reported acceptable ratio (CaP ranging 1.67–1.82) for synthesized NHA [13]. This increase in ratio could be as a result of formation of calcium hydroxide in addition to the hydroxyapatite after calcination [14]. The morphology and particle dispersion of the NHA powder synthesized at the optimum parameters is also depicted in figure 10. From figure 10a, the synthesized NHA was observed to disperse homogeneously. In figure 10b on the other hand, after the NHA powder was calcinated, the presence of porosity—an essential requirement for osteoconduction when dealing with bone implants, was observed [15–17]. Moreover, the particle shape of the synthesized NHA was determined using the TEM images obtained in figure 11. From the figure, the synthesized NHA powder before calcination (figure 11a) had needle-like shape, whereas after calcination the NHA particle shape changed to spherical-like (figure 11b). This is due to the increase in particle size from 45–65 to 75–140 nm after the NHA powder was calcinated. This is further complimented by the particle size distribution measured using zeta-sizer, where the particle size distribution ranged between 50–100 and 70–150 nm for the NHA before and after calcination, respectively. Hence, overall the synthesized NHA is indeed nano-sized that resembles the properties of the natural hydroxyapatite found in the bones; chemically and morphologically.

4. Conclusions

In this study, hydroxyapatite has been successfully synthesized using the precipitation method with the help of ultrasonication. The process parameters for synthesizing the NHA powder have been optimized using RSM based on 3 factors and 5 levels CCD design. Results revealed that the thermal stability and the particle size of the NHA powder synthesized were greatly influenced by the process parameters, especially the change in temperature. Additionally, a combination of lower temperature and lower amplitude or lower temperature and less ultrasonic time were also found to play a major role to produce intended NHA powder. The optimum process parameters were found to be 76°C, 24 min, and 61%, for temperature, ultrasonication time, and amplitude, respectively. The NHA powder synthesized at these optimized parameters which was further analyzed found to be in compliment with the predicted results from the RSM model.

Acknowledgement

We would like to acknowledge the financial support provided by the University of Nottingham, Malaysia Campus Research Grant (UNR30005) for this research.

References

[1] Suchanek W and Yoshimura M 1998 *J. Mater. Res.* **13** 94
[2] Hoque M E, Shehryar M and Islam K M N 2013 *J. Mater. Sci. Eng.* **2** 132
[3] Agrawal K, Singh G, Puri D and Prakash S 2011 *J. Miner. Mater. Charact. Eng.* **10** 727
[4] Xiao F, Ye J, Wang Y and Rao P 2005 *J. Mater. Sci.* **40** 5439

[5] Tang E, Huang M and Lim L 2003 *Int. J. Pharm.* **265** 103

[6] Gopi D, Govindaraju K, Victor C A P, Kavitha L and Rajendiran N 2008 *Spectrochim. Acta Part A: Mol. Biomol. Spectrosc.* **70** 1243

[7] Pang Y X and Bao X 2003 *J. Eur. Ceram. Soc.* **23** 1697

[8] Bezerra M A, Santelli R E, Oliveira E P, Villar L S and Escaleira L A 2008 *Talanta* **76** 965

[9] Scalera F, Gervaso F, Sanosh K, Sannino A and Licciulli A 2013 *Ceram. Int.* **39** 4839

[10] Eslami H, Solati-Hashjin M, Tahriri M and Bakhshi F 2010 *Mater. Sci.—Poland.* **28** 5

[11] Singh A 2012 *Bull. Mater. Sci.* **35** 1031

[12] Gross K A, Gross V and Berndt C C 1998 *J. Am. Ceram. Soc.* **81** 106

[13] Bonfield W and Gibson I R 2003 *Method for the preparation of carbonated hydroxyapatite compositions.* Google Patents

[14] Ansari M, Naghib S M, Moztarzadeh F and Salati A 2011 *Ceramics-Silikaty* **55** 123

[15] Rosa A L, Beloti M M and van Noort R 2003 *Dent. Mater.* **19** 768

[16] Annaz B, Hing K, Kayser M, Buckland T and Silvio L 2004 *J. Microsc.* **215** 100

[17] Okamoto M, Dohi Y, Ohgushi H, Shimaoka H, Ikeuchi M, Matsushima A *et al* 2006 *J. Mater. Sci.: Mater. Med.* **17** 327